

# The role of M cells and the long QT syndrome in cardiac arrhythmias: Simulation studies of reentrant excitations using a detailed electrophysiological model

Hervé Henry<sup>a)</sup> and Wouter-Jan Rappel

*Department of Physics, Center for Theoretical Biological Physics, University of California, San Diego, La Jolla, California 92093-0319*

(Received 9 July 2003; accepted 3 November 2003; published online 16 January 2004)

In this numerical study, we investigate the role of intrinsic heterogeneities of cardiac tissue due to M cells in the generation and maintenance of reentrant excitations using the detailed Luo–Rudy dynamic model. This model has been extended to include a description of the long QT 3 syndrome, and is studied in both one dimension, corresponding to a cable traversing the ventricular wall, and two dimensions, representing a transmural slice. We focus on two possible mechanisms for the generation of reentrant events. We first investigate if early-after-depolarizations occurring in M cells can initiate reentry. We find that, even for large values of the long QT strength, the electrotonic coupling between neighboring cells prevents early-after-depolarizations from creating a reentry. We then study whether M cell domains, with their slow repolarization, can function as wave blocks for premature stimuli. We find that the inclusion of an M cell domain can result in some cases in reentrant excitations and we determine the lifetime of the reentry as a function of the size and geometry of the domain and of the strength of the long QT syndrome. © 2004 American Institute of Physics. [DOI: 10.1063/1.1636272]

**Spatial heterogeneity of cardiac tissue causes cells to repolarize at different rates, leading to a dispersion of repolarization time. Dispersion of repolarization has been postulated to function as a substrate for reentry phenomena which occur when the propagation of the electric wave is blocked in one direction causing the wave front to curl and reenter the previously excited tissue. The ensuing incoherent electrical activity of the heart is thought to subsequently lead to ventricular fibrillation, the leading cause of sudden death in the industrialized world. In this numerical study, we investigate the role of intrinsic heterogeneities due to M cells in the generation and maintenance of reentrant excitations. These cells, located in the midmyocardium, exhibit a prolonged action potential duration and the resulting dispersion of repolarization is exacerbated in patients with the long QT syndrome. Using a detailed electrophysiological model, two previously postulated mechanisms are investigated: One in which the M cells create premature stimuli that lead to reentrant events and one in which the M cell domains function as wave blocks for electrically propagating waves originating, as usually, from the endocardium. We find that the first mechanism is unlikely to happen under the conditions we study, due to the strong electrotonic coupling that is normally present between neighboring cells. The second mechanism, on the other hand, can result in reentrant excitations. We determine the lifetime of the reentry as a function of the size and geometry of the domain, and of the strength of the long QT syndrome.**

## I. INTRODUCTION

Spatial heterogeneity of cardiac cells is commonly believed to play a major role in the generation and maintenance of arrhythmia. Both dynamic heterogeneity, where the dynamical properties of the homogeneous tissue are responsible for the heterogeneity,<sup>1–3</sup> and intrinsic heterogeneity, due, for instance, to the presence of different types of cells in the cardiac tissue, can result in cardiac cells that repolarize at different rates. The resulting dispersion of repolarization can lead to regions that block propagating waves and can, ultimately, result in reentry phenomena.

The focus of this study is intrinsic heterogeneities, which are present in a variety of forms. One of the most dramatic intrinsic heterogeneities is the presence of a layer of cells, M cells, roughly located in the middle of the myocardial wall.<sup>4,5</sup> This layer consists of cells that have distinct electrophysiological properties, most notably a prolonged action potential duration. The presence of these cells has been observed in many experimental studies and has been found in the ventricles of the dog,<sup>4</sup> guinea pig,<sup>6</sup> and human heart.<sup>7</sup> M cells may constitute up to 40% of the human left ventricular free wall<sup>7</sup> and the resulting action potential prolongation is most dramatic for isolated cells but remains substantial in wedge preparations where the M cells are coupled through gap junctions to the cells in the epi- and endocardium.<sup>8</sup> The dispersion becomes even more dramatic under the influence of cardiac drugs that prolong the action potential and/or in the presence of slow pacing.<sup>5</sup> The ion channels responsible for the prolongation of the action potential in M cells include primarily a smaller slow activating potassium current  $I_{Ks}$ , an augmented late sodium current  $I_{Na}$  and a larger sodium–calcium exchange current.<sup>9</sup>

It has been hypothesized that the resulting transmural

<sup>a)</sup>Electronic mail: hherve@physics.ucsd.edu

dispersion plays a major role in the initiation and maintenance of reentry.<sup>10</sup> In particular, the role of M cells in the initiation of torsade de pointes, a polymorphic ventricular tachycardia, in patients with the long QT syndrome has recently received considerable attention.<sup>11</sup> The long QT syndrome is characterized by a prolonged ventricular repolarization and is associated with a high risk of sudden cardiac death. It manifests itself as an abnormally long QT interval in the ECG and can be either congenital, idiopathic or acquired (for a review see Ref. 12). Several forms of long QT syndromes with different cellular mechanisms and clinical characteristics have been identified. Nearly all cardiac events in patients with long QT 1, associated with a reduced  $I_{Ks}$ , are initiated during increased sympathetic activation induced by physical or emotional stress.<sup>13,14</sup> On the other hand, in patients with long QT 2, characterized by a decrease in  $I_{Kr}$ , and long QT 3, corresponding to a late  $I_{Na}$ , cardiac events occur most often during rest or sleep.<sup>13</sup>

Several possible mechanisms linking M cells and dispersion of repolarization with cardiac arrhythmias have been postulated. In one, M cells develop early-after-depolarizations, which are characterized by a depolarization at the end of the action potential plateau. This depolarization could then create a premature stimulus via the electrotonic interaction with neighboring cells. This premature stimulus will be partially blocked by the M cell domain but can initiate a wave in other directions. Once the repolarization is complete, this wave can reenter the M cell zone, leading to a classic figure-of-eight reentry.<sup>15</sup> Crucial to this mechanism is the ability for the early-after-depolarizations to excite neighboring cells despite electrotonic effects that will tend to smooth out steep gradients.

In another possible mechanism, the dispersion of repolarization due to M cells creates regions with delayed repolarization that act as conduction blocks for subsequent waves. Under suitable conditions, the dispersion of repolarization can then lead to partial wave block and reentry. This scenario has recently been shown to be plausible in a canine wedge preparation of the left ventricle.<sup>11</sup> In this study, a transmural cross section of the wedge was visualized via voltage sensitive dyes and long QT 2 conditions were realized pharmacologically by adding the  $I_{Kr}$  blocker d-sotalol.<sup>16</sup> This led to a marked increase in dispersion of repolarization and the presence of distinct islands of M cells, which resulted in areas with steep spatial gradients of repolarization. When the wedge was paced under bradycardic conditions from the endocardium, followed by a premature stimulus delivered at a short coupling interval (time interval between the premature stimulus and the previous, regular stimulus), the islands were found to function as conduction blocks and torsade de pointes ensued. The underlying mechanism of the resulting arrhythmia was demonstrated to be sustained intramural reentrant excitations.

Only a limited number of numerical studies investigating long QT syndromes, dispersion of repolarizations and its role in arrhythmias has been undertaken. Work by Rudy and colleagues investigated long QT syndrome in isolated cells<sup>17,18</sup> and strands of cells with embedded domains of M cells<sup>19,20</sup> but did not address the role of M cells in the initiation of

reentry. Clayton *et al.*<sup>21</sup> studied the size of the vulnerable window, defined as the time interval for which a premature stimulus initiates a unidirectional wave, in homogeneous strands of tissue. They found that long QT conditions did not increase this size measurably. However, they did not investigate propagation block in strands having domains consisting of electrophysiologically different cells. They also investigated the tip trajectory in numerical models for long-QT 1, 2, and 3, using a relatively large square homogeneous domain but did not study the initiation of reentrant excitation.

In this paper, we use a detailed electrophysiological model<sup>22</sup> to investigate the two possible mechanisms detailed above. We first study if normally coupled tissue can generate unidirectional waves in one-dimensional (1D) strands of tissue. We then determine under what conditions a domain of M cells will block propagation in a 1D cable. We finally determine under what conditions a two-dimensional (2D) sheet of tissue containing a layer of M cells will lead to reentrant excitation.

## II. THE MODEL

To describe the electrophysiological properties of the cardiac cell we use the Luo–Rudy dynamic (LRd) model.<sup>22,23</sup> The dynamics of the tissue is described by the reaction-diffusion equation

$$\frac{\partial V}{\partial t} = \frac{1}{C_m \rho S_v} \nabla^2 V - \frac{I_{ion}}{C_m}, \quad (1)$$

where  $V$  (mV) is the membrane potential,  $C_m$  ( $\mu\text{F cm}^{-2}$ ) is the membrane capacitance,  $\rho$  ( $\Omega\text{cm}$ ) is the bulk resistivity,  $S_v$  ( $\text{cm}^{-1}$ ) is the surface to volume ratio and  $\nabla^2$  is the Laplacian operator. The combination of  $1/C_m \rho S_v$  gives the diffusion constant  $D$ , which we have taken to be  $D = 1/C_m \rho S_v = 0.11 \text{ cm}^2/\text{s}$  resulting in a planar wave speed of approximately 17 cm/s. This speed is consistent with experimentally observed wavespeeds in canine ventricles when measured perpendicular to fibers.<sup>24</sup> As is the case for all electrophysiological models, the details of the LRd model are contained in the description of the total ionic current  $I_{ion}$  ( $\mu\text{A cm}^{-2}$ ) flowing through the cardiac cell membrane. In contrast to earlier models, which describe only a small number of ionic currents, the LRd model and other often so-called “second generation” models attempt to incorporate as many significant currents as possible, including a more complete description of intracellular calcium dynamics.

Our choice of the LRd model was motivated by several considerations. First, all other existing models we tested, including the first generation Luo–Rudy<sup>25</sup> and Beeler–Reuter<sup>26</sup> models and the second generation model of Fox *et al.*,<sup>27</sup> exhibited spiral cores that were typically comparable to or larger than the computational domain, taken to be typical of human ventricles. Thus, these models are not suitable to investigate sustained reentry in our computations. Second, we are interested in modifying specific currents that are responsible for the distinct properties of M cells and that play a role in the long QT syndrome (see below). The LRd model, being a second generation model, allows us to change these currents directly.

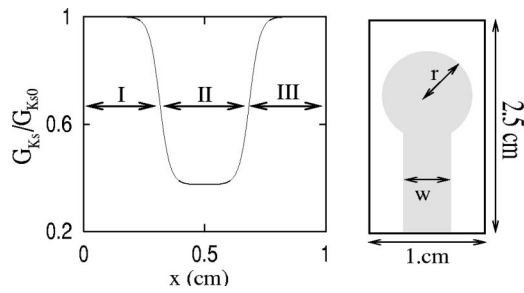


FIG. 1. (a) Typical profile of the maximal conductance of  $I_{Ks}$ ,  $G_{Ks}$ , used in the numerical studies of a cable. The conductance is shown normalized by the maximal conductance in normal tissue,  $G_{Ks0}$ . The cable consists of a region of width  $w$  with a reduced  $G_{Ks}$  (II) corresponding to M cells, sandwiched between two equally sized domains of normal tissue (I and III). (b) The geometry considered in our 2D simulations, consisting of a region of M cells, shaded in gray, surrounded by normal tissue. As in the cable, the M cells are modeled via the reduction of  $G_{Ks}$  and the transition between the different domains is taken to be smooth.

Since M cells are predominantly present in the midmyocardium, we focus here on the effects of regional heterogeneities in transmural geometries. Furthermore, since the transmural wedge experiment in Ref. 11 suggests that, at least in the initial stages, the reentry caused by the long QT syndrome is a 2D phenomenon we have limited ourselves to tissue sheets that represent thin transmural wedges. We have taken the transmural dimension to be 1 cm, while the other dimension is taken to be 2.5 cm. Also, we found it useful to investigate the behavior of the tissue in a 1D cable that can be thought of as a straight line traversing the myocardial wall and perpendicular to the endo- and epicardial walls. In all simulations, we have taken a spatial discretization of 0.008 cm and a time step of 0.02 ms. We have verified that using smaller time and space steps did not significantly modify the quantitative results.

Spatial heterogeneity was introduced by subdividing the cable into three domains [see Fig. 1(a)]. Since we focus here primarily on the role of the M cell domain, we have chosen two outer domains that have equal length and identical electrophysiological properties. This is, of course, a simplification as the endo- and epicardium can have different electrophysiological properties.<sup>9</sup> However, in the canine wedge preparation, the action potential durations of the epi- and endocardial cells were only minimally different.<sup>11</sup> The middle domain consists of a region of M cells, which, electrophysiologically, were modeled by decreasing the value of the maximum conductance  $G_{Ks}$  of the slow activating potassium current  $I_{Ks}$ . We tuned the value of  $G_{Ks}$  such that the epi- and endocardial cells and the M cells had an action potential that correspond to the experimental findings in Ref. 11. Specifically, we took the normal tissue to have a maximal conductance  $G_{Ks0}$  that was a factor of 1.5 larger than the original value in the LRd model while the maximal conductance  $G_{Ks1}$  in the M cells was chosen as  $G_{Ks1} = 0.375G_{Ks0}$ .

The transition between the two regions was made smooth by employing a simple sigmoidal function for  $G_{Ks}$  [see Fig. 1(a) and supplemental material]. The two-dimensional (2D) geometry consists of a transmural slice of the myocardial wall containing a strip of M cells. Of course,

it is impossible to initiate reentry via uniform pacing of the entire endocardium if the computational domain is invariant under translation along the endocardium [the vertical direction in Fig. 1(b)]. Thus, to break the symmetry we have chosen to use an M cell layer consisting of a strip of width  $w$  that starts at one boundary and ends with a “bubble” with radius  $r$  at the other end [see Fig. 1(b)]. Evidence for inhomogeneous distributions of M cells can be seen in Ref. 11 where the repolarization maps show distinct islands of slower repolarization, presumably corresponding to M cell domains. As in the 1D cable, the transition between the different domains was made smooth.

We will focus here mostly on long QT 3, which is characterized by an incomplete inactivation of the sodium current  $I_{Na}$  and which leads to an abnormally prolonged action potential, particularly in M cells. To model the  $I_{Na}$  channel and to allow a description of the long QT 3 mutant we have adopted the strategy of Clancy and Rudy and have replaced  $I_{Na}$  in the LRd model with a Markovian description.<sup>28</sup> That is, instead of calculating the opening and closing of the fast sodium channel using gating variables that are deterministic functions of the membrane potential, we describe this channel using a collection of open, closed and inactivation states. The transition rates between these states are dynamically calculated and are functions of  $V$ . In addition to the background mode, also present in wild type cells, mutant cells have a burst mode which does not include inactivation states. When the channel is in this burst mode, the inactivation transiently fails, leading to a leak current and a prolonged action potential.

To simplify the original model for  $I_{Na}$ <sup>28</sup> and its subsequent refinement,<sup>29</sup> and to render our computations more efficient, we have changed the original Markovian model. More details of this modification can be found in the supplemental material. In essence, the simplification uses the existence of two distinct timescales of the  $I_{Na}$  channel: A short time scale on the order of a single action potential and a much longer timescale on the order of multiple action potentials. Using these two timescales the Markov model can be reduced to an equation for  $I_{Na}$  which is similar to the original formulation in the LRd model supplemented by a dynamical equation which describes the fraction of channels in the burst mode. Numerical checks, presented in the supplemental material, show that the reduced description accurately reproduces the leak current. Furthermore, we have verified that action potentials generated with the simplified model do not differ significantly from those generated using the full model.

The simplification of  $I_{Na}$ , along with the geometry of our computational domain, lead to several adjustable parameters in our simulations. First, the strength of the long QT syndrome can be changed via a single dimensionless parameter  $\mu$ . It is a measure of the fraction of mutant cells (see Appendix) and is equal to zero in the case of normal cells. Second, the width of the M cell layer  $w$  can be changed. Finally, in 2D we have the additional parameter  $r$ , the radius of the disk at the end of the M cell layer. Notice that the minimal value of  $r$ ,  $r = w/2$ , corresponds to a strip with a rounded edge.

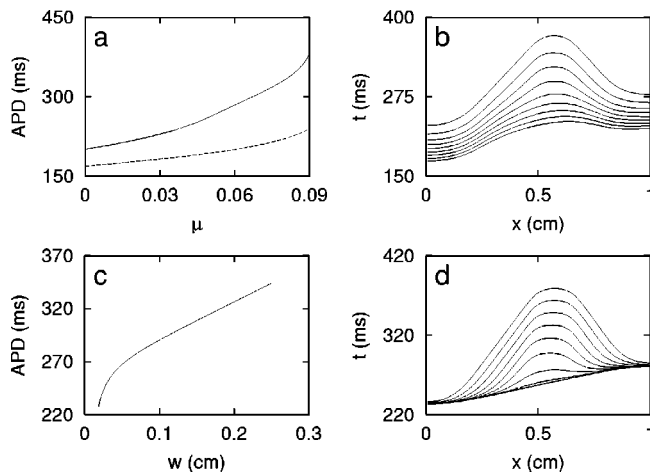


FIG. 2. (a) Action potential duration at a basic cycle length of 1000 ms as a function of the strength of the leak  $I_{Na}$ ,  $\mu$ , at the midpoint of a cable with (solid line,  $w=0.48$  cm) and without an M cell domain (dashed line). (b) Corresponding repolarization times for different values of  $\mu$  varying from 0 (bottom line) to 0.09 with steps of 0.01. (c) Action potential duration at the midpoint of the cable as a function of the width of the M cell domain (basic cycle length = 1000 ms and  $\mu=0.08$ ). (d) Corresponding repolarization time for different widths of the M cells region ranging from a homogeneous cable ( $w=0$  cm and bottom line) to a domain of width  $w=0.48$  cm with increments of 0.06 cm.

### III. RESULTS

#### A. One dimension

We first quantified the effect of the size of the M cell domain  $w$  and of the long QT syndrome strength  $\mu$  on action potential duration in a cable. For this, we stimulated the cable at one end with a fixed basic cycle length of 1000 ms for 40 s. We then measured the action potential duration in the cell at the midpoint of the cable (and thus at the midpoint of the M cell domain) and at the end of the cable. In Fig. 2(a) we plot the action potential duration as a function of  $\mu$  at the midpoint of a cable with (solid line,  $w=0.48$  cm) and without an M cell domain (dashed line,  $w=0.0$  cm). Figure 2(b) shows the corresponding repolarization times along the cable, measured as the time interval between the stimulus and the time at which the membrane potential has repolarized to  $V = -70$  mV. As expected, increasing the long QT syndrome strength results in an increase in action potential durations. Since the action potential duration in M cells is more strongly affected by an increase in  $\mu$ , higher values of  $\mu$  result in an increased dispersion of repolarization time in the tissue. In Fig. 2(c) we show the action potential durations at the midpoint of the heterogeneous cable as a function of  $w$  for  $\mu=0.08$ , the long QT syndrome strength employed in most of this study. The corresponding repolarization times can be found in Fig. 2(d). The action potential duration of points well into the normal tissue are hardly affected by increasing  $\mu$  while the midpoint of the cable displays a marked increase in action potential duration when  $w$  is increased. The action potential durations computed numerically here for  $\mu=0$  and  $\mu=0.08$  are similar to the ones observed in Ref. 11 when the wedge was paced under bradycardic conditions with and without d-sotalol, respectively.

The shape of the action potential at different sites of the

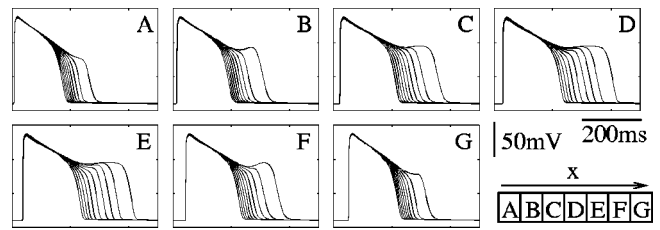


FIG. 3. Action potentials at different positions along a cable of length 1 cm for increasing values of  $\mu$  from 0 (shortest action potential) to 0.09 (longest action potential) with steps of 0.01. The domain of M cells has a width of  $w=0.48$  cm and corresponds to the region (c)–(e), while the transition regions are (b) and (f). The basic cycle length is 1000 ms, the horizontal bar corresponds to 200 ms and the vertical bar corresponds to 50 mV.

cable can be seen in Fig. 3. Here, we have divided the cable into seven subdomains and have plotted the action potential for each subdomain for a fixed stimulation period of 1000 ms and varying long QT syndrome strength. The domain of M cells has a width of  $w=0.48$  cm and corresponds to Figs. 3(c)–3(e). It can clearly be seen that the long QT syndrome has a more dramatic effect on the M cells [Fig. 3(d)] than on normal cells [Figs. 3(a) and 3(g)]. Also note that due to the symmetry breaking introduced by the pacing at the left end of the cable, the action potentials are longer at the right boundary of the M cell domain [Fig. 3(f)] than at the left boundary [Fig. 3(b)].

Next, we investigated if the presence of M cells could provoke early after depolarizations and waves propagating unidirectionally in our cable. We first verified that single M cells exhibit early after depolarizations, defined as an increase in the membrane potential during the plateau phase of the action potential. We found that these early after depolarizations are present for a relatively wide range of parameters and pacing protocols and have an amplitude that is consistent with experimental findings. This is shown in Fig. 4(a1) where we plot, as a solid line, three subsequent action potentials for an isolated M cell with  $\mu=0.06$ . In contrast, an isolated epi- or endocardial cell, paced at the same basic cycle length of 1000 ms, does not exhibit early after depolarizations (dashed line).

Having established the presence of early after depolarizations in isolated cells, we next considered a cable containing a domain of M cells. In Fig. 4(a2), we show the action potential in a cable consisting of cells identical to the ones of Fig. 4(a1). The solid line represents the membrane potential at the middle of the M cell domain ( $w=0.48$  cm), while the dashed line represents the membrane potential in the middle of the epicardial domain. The early after depolarizations, present in the isolated cells, have now disappeared due to electrotonic effects. We found qualitatively similar results for different basic cycle lengths, long QT strengths and widths of the M cell domain: Early after depolarizations provoked in single M cells were always found to be suppressed by electrotonic effects once the cells were inserted in a cable containing an M cell domain sandwiched between an endo- and epicardial domain.

In fact, we found that, for the model used here, the only possible way to generate an early after depolarization that travels along a homogeneously coupled cable is to either

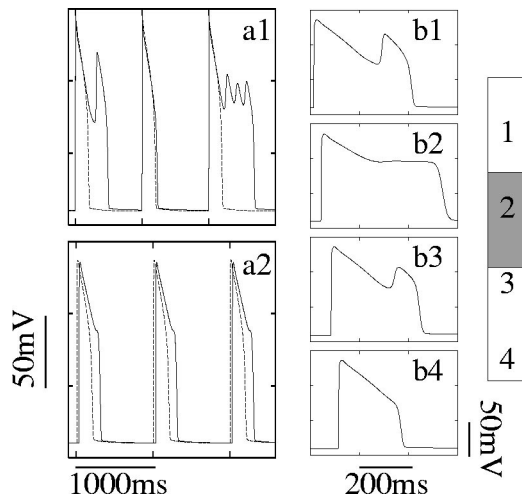


FIG. 4. (a1) The membrane potential for a single isolated M cell (solid line) for a long QT strength  $\mu=0.06$ , along with the membrane potential for a single isolated epi- or endocardial cell (dashed line). The cell is paced with a basic cycle length equal to 1000 ms. (a2) Membrane potential at different positions along our inhomogeneous cable ( $w=0.48$  cm) consisting of cells used in (a1). The solid line correspond to the midpoint of the M cell domain, while the dashed line correspond to the middle of the epicardial domain. (b1)–(b4) The membrane potential at four different locations along the cable, as indicated by the graph on the right. The M cell domain ( $w=0.48$  cm) is shaded gray and the cable ( $\mu=0.09$ ) is paced using a basic cycle length of 1000 ms, followed by a stimulus with a coupling interval of 2000 ms.

change the pacing protocol or to increase the long QT strength significantly. Both scenarios lead to early after depolarizations that are already present in the endocardial domain. An example is shown in In Fig. 4(b) where we have plotted the action potential at four different locations along the cable as indicated in the figure. The cable was paced at a constant basic cycle length of 1000 ms, followed by a stimulus with coupling interval of 2000 ms. The endocardial domain now generates an early after depolarization with a significant amplitude that is able to travel through the M cell domain into the epicardial domain. However, the early after depolarization is propagating with a smaller speed that the repolarization wave and disappears before reaching the end of the cable. Thus, in conclusion, under normal coupling conditions, the diffusive term in Eq. (1) always leads to considerable dissipation of the membrane potential, which prevents the early after depolarizations from stimulating neighboring tissue.

Some studies have suggested that a discontinuity in conductivity exists between the M cell domain and the epicardium, leading to inhomogeneous coupling.<sup>8</sup> It is possible that the inclusion of such inhomogeneous coupling, as shown in other modeling studies that investigated the propagation from the Purkinje fibers (specialized fibers that rapidly transmit impulses from the atrioventricular node to the ventricles) to the myocardium,<sup>30,31</sup> allows for unidirectional conduction. However, we found that propagation provoked by early after depolarizations in our model was only possible when we altered the conductance significantly. Specifically, we found that we had to reduce the conductance by at least a factor of 10, which is much more than the factor of three reported in

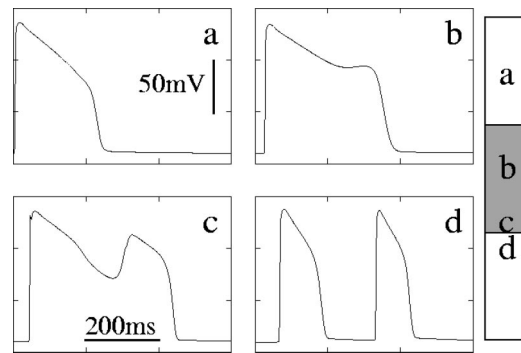


FIG. 5. Action potentials at different positions along a cable of length 1 cm shown on the right. The shaded M cell domain has width  $w=0.6$  cm and the cable ( $\mu=0.08$ ) is paced with basic cycle length of 1000 ms, followed by a stimulus with coupling interval of 1200 ms. The maximal conductance  $G_{Ks}$  of the slow activating potassium current was increased by a factor of two in the epicardial domain. The resistance between the last gridpoint of the M cell domain and the first gridpoint of the epicardium was abruptly increased by a factor of 13 and returned to normal over the following 10 gridpoints.

Ref. 8. An example is shown in Fig. 5 where we have plotted the membrane potential at four different locations in the cable, as indicated in the figure. An early after depolarization appears in the M cell domain (b) as the coupling interval is increased. This early after depolarization becomes more pronounced at the boundary of the M cell domain and the epicardium, where the resistance is increased by a factor of 13. The increased resistance allows the epicardium to repolarize and the early after depolarization eventually creates an extra stimulus in the epicardium.

These results suggest that the first arrhythmic mechanism described in the Introduction is unlikely to occur in the

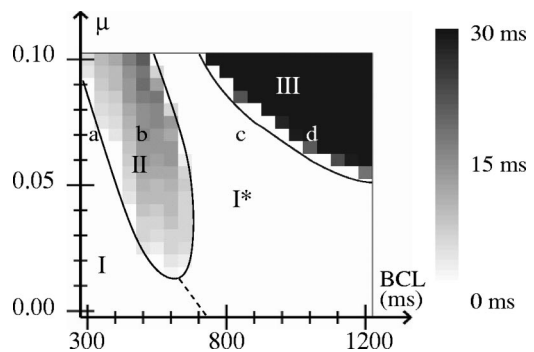


FIG. 6. Phase diagram of the response of a cable paced at a regular basic cycle length (BCL) to a premature stimulus in the presence of a M cell domain of width 0.48 cm and of varying long QT syndrome strength. In regions I and I\* no conduction block occurs: A wave that has begun to propagate will propagate through the cable. In region I the wave speed in the M cell domain is similar to the wave speed in the normal domain while in region I\* the wave in the M cell domain slows down considerably before resuming normal propagation. The dashed line is a guide to the eye to separate the two different regions. Regions II and III correspond to two different types of conduction block. In region II the normally propagating wave reaches the M cell region and fails to propagate almost immediately. Region III, on the other hand, corresponds to conduction block in which the wave is able to enter the M cell domain, where it propagates with a significantly decreased wave speed before failing to propagate. The size of the window of coupling intervals which lead to conduction block in regions II and III is indicated by a gray scale, with white being the smallest range and black being the largest range.

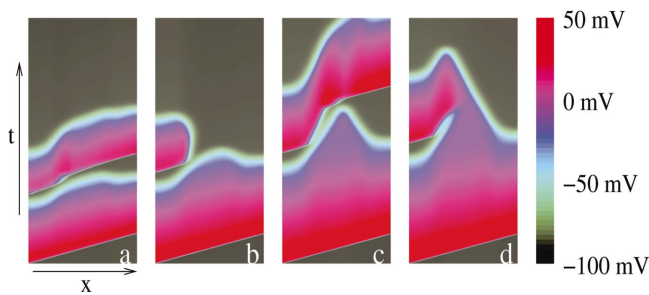


FIG. 7. (Color) Space–time diagrams of the transmembrane potential of a cable of length 1 cm that includes an M cell domain of width  $w=0.48$  cm and long QT strength  $\mu=0.07$ . The cable is paced at the left end with constant basic cycle length for 10 s, after which a premature stimulus of varying coupling intervals is given. The color code used is shown by the colorbar on the right. The four figures (a)–(d) correspond to the points marked (a)–(d) in Fig. 6 and are typical of the dynamics in the four different regions in that figure. (a) Dynamics representative of region I in Fig. 6: The premature stimulus (coupling interval=140 ms) propagates through the M cell domain with almost the same speed (basic cycle length=300 ms). (b) Dynamics representative of region II in Fig. 6: The wave is blocked immediately when entered the M cell domain (basic cycle length=500 ms and coupling interval=184 ms). For this basic cycle length, the conduction block window was fairly small (15 ms) with conduction block occurring for a coupling interval between 170 and 185 ms. (c) Dynamics representative of region I\* in Fig. 6: Due to the slow repolarization of the M cells the wave speed is significantly decreased when entering the M cell domain. The speed increases again when the wave can propagate freely through the repolarized medium (basic cycle length=800 ms and coupling interval=224 ms). (d) Dynamics representative of region III in Fig. 6: The wave speed decreases dramatically upon entering the M cell domain. However, unlike (c), normal propagation is unable to resume and the wave is blocked (basic cycle length=1000 ms and coupling interval=245 ms). For this stimulation period, we found a conduction block window of 72 ms with conduction block occurring for a coupling interval between 225 and 297 ms.

model we consider here. To study the second mechanism, we recall that this scenario predicts the blocking of a wavefront by the remnants of previous stimuli. To investigate the possibility of a wave block created by the M cell domain, we again paced the cable at one end with a fixed period. After 40 cycles, we delivered a premature stimulus to the same end of the cable and varied the coupling interval between the last of the regular cycles and the premature stimulus. Conduction block was defined as an inability to propagate through the M cell domain to the opposite end of the cable. The experiment was repeated for different basic cycle lengths and the conduction block window, the range of coupling intervals that resulted in a conduction block, was determined.

We found a rich set of possible dynamics that is summarized in Fig. 6 where we have plotted our findings in the basic cycle length (BCL) vs strength of the long QT syndrome ( $\mu$ ) phase space. For wild type cells, i.e.,  $\mu=0$ , the presence of the M cells domain does not lead to any conduction block. However, qualitatively different wave propagations are present. For small pacing periods, the premature wave travels through the M cell region with almost unchanged speed. This behavior is demonstrated in Fig. 7(a) which shows a color-coded space–time plot of the membrane voltage. The parameter values for Fig. 7(a) correspond to the point marked a in Fig. 6. Its behavior is typical of all points in region I in Fig. 6. For longer pacing periods, the wave front slows down significantly when entering the M cell re-

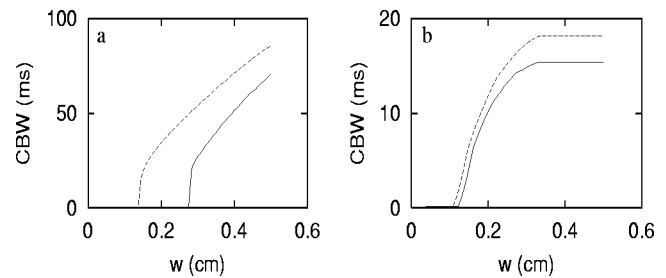


FIG. 8. The conduction block window duration (CBW) as a function of the width of the M cell domain for  $\mu=0.07$  (dashed lines) and  $\mu=0.08$  (solid lines) for a basic cycle length of 1000 ms (a) and 500 ms (b). Note the different scales of the CBW axis.

gion. After coming almost completely to a stop, with typical wave speeds found to be around 4 cm/s, the wave resumes its original speed and propagates into the epicardium. This slow-down-and-go behavior is demonstrated in Fig. 7(c), corresponding to point c in Fig. 6, and is representative of the points in the region labeled I\* in Fig. 6.

For sufficiently large values of  $\mu$ , conduction block occurs (regions II and III in Fig. 6). Two qualitatively different types of conduction block are observed. In region II, the wave penetrates the M cell domain only slightly before being blocked. A space–time plot of point b within region II is shown in Fig. 7(b). The conduction block window for points in region II is rather small, typically less than 20 ms. This range is indicated in Fig. 6 on a linear gray scale with white corresponding to small conduction block windows and black corresponding to large ones ( $>30$  ms). The conduction block window for point b was found to be 15 ms.

The second type of conduction block can be found in region III and is shown in Fig. 7(d). A wave front enters the M cell domain, reduces its speed significantly and is subsequently blocked. The conduction block window for this region is much larger than for region II. For example, the conduction block window for point d is 72 ms. This is also shown in Fig. 8 where we have plotted the conduction block window as a function of the width of the M cell domain for two different values of the long QT strength and for two different values of the pacing period. For both regions II and III the conduction block windows increases as  $w$  is increased. We have also investigated the location of the boundaries of the regions in Fig. 6 for different  $w$ . Increasing  $w$  did not significantly increase the size of any of the regions, while decreasing  $w$  reduced the size of regions II and III. Of course, for  $w=0$  no conduction block occurs and both regions II and III are absent in the phase diagram.

In most of region III the behavior of the wave as a function of the coupling interval for fixed basic cycle length and  $\mu$  can be summarized as follows: For large coupling intervals, the wave is able to propagate normally through the M cell domain. Upon decreasing the coupling interval the wave slows down significantly inside the M cell domain. Below a critical coupling interval conduction stops within the M cell domain. Finally, after decreasing the coupling interval even further, propagation fails already in the epicardial domain [domain I in Fig. 1(a)]. Close to the boundary of region III with region I\* a different behavior is observed. Again, for

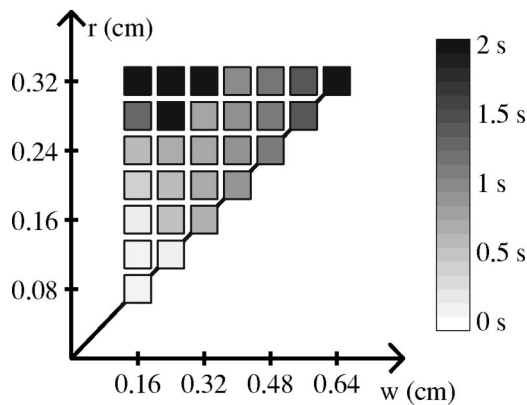


FIG. 9. Phase diagram: Duration of the reentry as a function of the two parameters governing the geometry of the 2D sheet: the width of the M cell region ( $w$ ) and the radius of the bubble ( $r$ ). The grayscale indicates the duration as shown by the bar on the right (units are in seconds). A relatively sharp transition occurs between a regime for which reentries last at most around 1 s and a regime for which reentries last for more than 2 s and are pinned by the bubble (black squares).

large coupling intervals the wave is able to propagate normally through the M cell domain. For smaller coupling intervals the wave slows down, and below a first critical coupling interval, propagation fails. Upon further decreasing the coupling interval, however, wave propagation resumes, characterized by a slowly propagating front within the M cell domain. Below a second critical coupling interval propagation fails in the epicardial domain. We will leave the discussion of this behavior to future studies.

In summary, our 1D results show that, for properly timed premature stimuli and sufficiently large values of  $\mu$ , the presence of a domain of M cells can create a conduction block. Furthermore, early-after-depolarizations were observed to develop within the M cell domain. However, in our numerical experiments, they are unable to excite already repolarized neighboring tissue due to electrotonic interactions. Thus, reentrant excitations will not be generated in our model via the first mechanism and in our 2D simulations we will exclusively focus on the second mechanism.

## B. Two dimensions

To investigate whether the second mechanism could lead to reentrant excitation in 2D we performed an extensive numerical study of a transmural sheet, shown in Fig. 1(b). Our simulation protocol was chosen to reduce the computational cost while minimizing any drift in the action potential duration. For this, we first divide the 2D sheet into 1D cables running from the endo- to epicardium. These cables are then paced from the endocardial end for 40 s, after which the sheet is reassembled. Then, the entire sheet is paced for a further 10 s by stimulating the entire endocardium. This is finally followed by a premature stimulus with a varying coupling interval. Rather than choosing the premature stimulus at the epicardium as was done in Ref. 11, we used a stimulus originating from the entire endocardium. This can be thought of as a premature stimulus coming from the Purkinje fiber.<sup>31</sup>

Our main result is summarized in Fig. 9 where we show the length of reentry, measured in seconds, as a function of

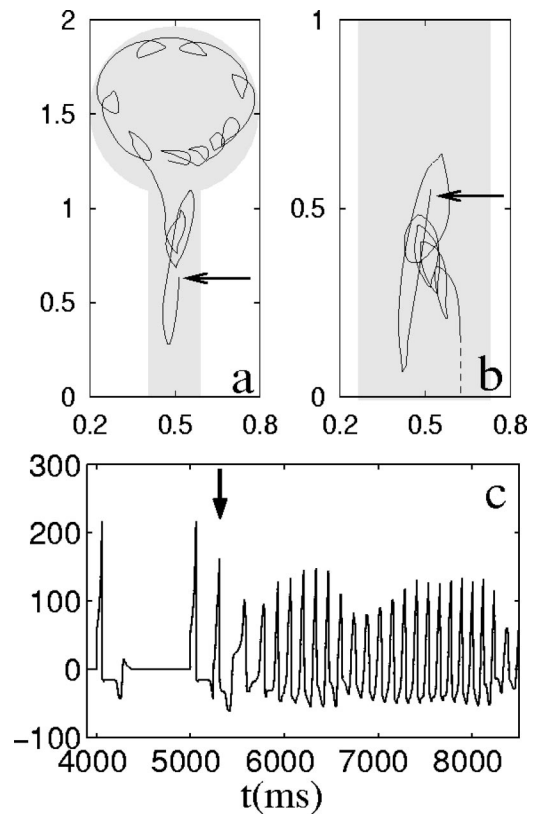


FIG. 10. Spiral tip trajectories for  $w=0.48$  cm and  $r=0.24$  cm (a) and  $w=0.24$  cm,  $r=0.32$  cm (b). The M cell domain is lightly shaded and the long QT syndrome strength is  $\mu=0.08$ . In both cases, the start of the tip trajectory is indicated by an arrow and the initial stage of the reentrant excitation is shown. In (a), the dashed line is used as a guide to the eye in order to show that the spiral ends up leaving the sheet. The size of the tissue sheet is  $1\text{ cm} \times 2.5\text{ cm}$ . (c) Simulated pseudo-ECG corresponding to the reentry shown in (b), showing the fourth and fifth regular beat and the premature stimulus indicated by the arrow.

the two geometry parameters,  $w$  and  $r$ , for fixed long QT syndrome strength  $\mu=0.08$ . Of course, the duration of reentry is also dependent on the coupling interval (see below and Fig. 12) and to determine its value, we varied the coupling interval in steps of 1 ms and measured the duration of reentry for the five coupling intervals that produced the longest lived reentrant excitations. The average of these five events is shown in Fig. 9 using a gray scale with white corresponding to short-lived reentry and black corresponding to long-lived reentry. Note that the diagonal corresponds to a strip with a rounded edge.

From the figure, one can see that reentry that lasts longer than 1 s requires a sufficiently large M cell domain. This can be accomplished by either having a wide strip ( $w > 0.48$  cm), or having a large bubble ( $r > 0.28$  cm for  $w = 0.24$  cm). These two cases, however, result in qualitatively different reentrant patterns. A typical spiral tip trajectory for a wide, rounded-edged, strip is shown in Fig. 10(a). The tip was calculated every 1 ms using the intersection of the isocountour  $V = -30$  mV and the line defined by  $h = 0.5$ , where  $h$  is the inactivation gate of the sodium channel.<sup>21</sup> The initial phase of the reentry is not shown and the first point of the tip trajectory is marked by the arrow. The spiral eventually drifts

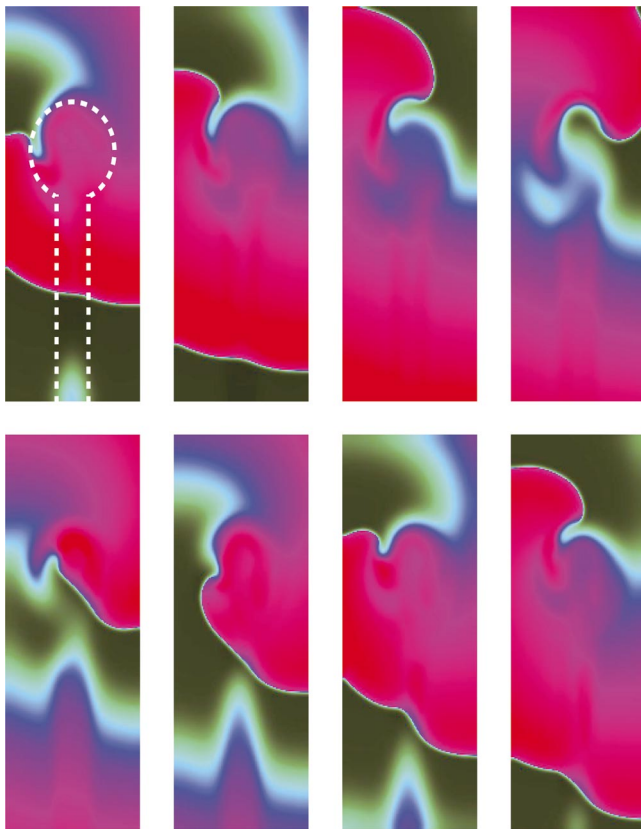


FIG. 11. (Color) Color plots of the membrane potential of the reentrant excitation of Fig. 10(b). The M cell domain is indicated by the white dashed line. The plots are taken 25 ms apart and start 1 s after the application of the premature stimulus. The first one is in the upper left hand corner while the last one is in the lower right hand corner. The color scale is identical to the one employed in Fig. 7. Parameter values:  $\mu=0.08$ ,  $w=0.24$  cm,  $r=0.32$  cm, and a physical domain of  $1\text{ cm}\times 2.5\text{ cm}$ .

out of the computational domain, which is indicated by the dashed line. The total trajectory in Fig. 10(a) represents 1 s and approximately five spiral rotations.

The tip trajectory in the case of a large bubble is shown in Fig. 10(b) where we again have omitted the initial part of the reentrant excitation and marked the first point of the trajectory with an arrow. Here, the spiral tip becomes pinned to the bubble, leading to long lasting reentry. A qualitative similar picture was found in a numerical study of a tissue sheet with a central ischemic region.<sup>32</sup> The spiral tip is plotted for roughly 2 s and 10 spiral rotations in Fig. 10(b). The corresponding simulated pseudo-ECG, using the algorithm in Ref. 33, is shown in Fig. 10(c). In this figure, we have included the two regular preceding beats and have indicated the premature stimulus by an arrow. The polymorphic undulating ECG is suggestive of torsade de pointes. Finally, the reentrant excitation of Fig. 10(b) is also plotted in Fig. 11 where we show the activation of the tissue every 25 ms using the color scale of Fig. 7.

Since reentry is caused by the partial blocking of the premature stimulus, we found a good correlation between the range of coupling intervals that leads to reentry and the range of coupling intervals that leads to a 1D conduction block. This is illustrated in Fig. 12 where we have plotted the length of reentry as a function of the coupling interval for  $\mu$

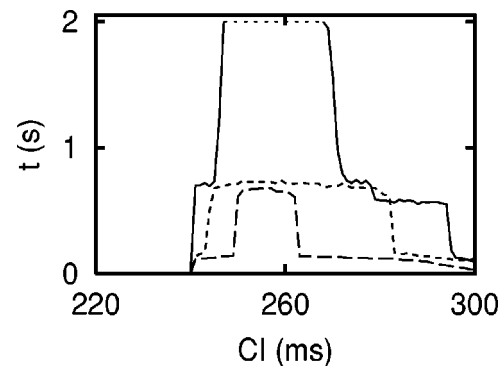


FIG. 12. The length of reentry as a function of coupling interval for the transmural sheet with  $\mu=0.08$ , basic cycle length=1000 ms,  $w=0.32$  cm and three different values of  $r$  [0.32 cm (solid), 0.24 cm (short dashed), and 0.16 cm (long dashed)]. Reentrant excitations for  $r=0.32$  cm (solid line) that were characterized by a pinning to the bubble and that persisted throughout the duration of our numerical simulations (2 s) are indicated by the dotted line.

$=0.08$ ,  $w=0.32$  cm, and three different values of  $r$ . For these parameter values, the 1D cable simulations reveal a conduction block for coupling intervals between 240 and 300 ms. In 2D, the onset of reentry occurs for a coupling interval of 240 ms, as can be seen in Fig. 12 and no reentry is observed for coupling intervals larger than 300 ms. As already mentioned before, a larger bubble size leads to a more sustained reentry. In fact, for large bubbles, the spiral tip becomes attached to the bubble, resulting in reentry persisting throughout the full duration of our numerical simulations (2 s). These points are indicated by the dotted line in Fig. 12.

#### IV. DISCUSSION

We have presented a numerical study of the role of a particular type of spatial heterogeneity in cardiac tissue in the initiation and maintenance of reentrant excitations. Specifically, we have addressed the role of M cells, located in the midmyocardium. The prolonged action potential of M cells leads to dispersion of repolarization which is increased significantly in patients with the long QT syndrome. We have focused on the long QT 3 syndrome which is marked by an increase in the late  $I_{Na}$  and have investigated two previously proposed mechanisms, using numerical simulations of inhomogeneous tissue cables and sheets.

The first mechanism proposes that early after depolarizations in the M cell domain leads to premature stimuli in surrounding tissue. However, our numerical results show that under normal electrotonic coupling, the late sodium current is not sufficiently strong to induce an excitation in neighboring points. Typical currents that are responsible for the generation of early after depolarizations are fairly small.<sup>34</sup> For example, in the case studied here, the late  $I_{Na}$  current is on the order of  $2-4\ \mu\text{Acm}^{-2}$  while in long QT 1 and long QT 2, the respective reduction of  $I_{Ks}$  and  $I_{Kr}$  is on the order of  $1\ \mu\text{Acm}^{-2}$ . Furthermore, the L type calcium current involved in the generation of early after depolarizations is roughly of the same magnitude. This should be compared to the strength of the injection current needed to induce a counter propagating wave in a cable with  $\mu=0$ . Numerically,

we find that the necessary injection current is approximately an order of magnitude larger ( $\sim 30 \mu\text{Acm}^{-2}$ ). It is therefore perhaps not a surprise that the inclusion of a leak current in  $I_{\text{Na}}$  is not sufficient to create a wave propagating in the unidirectional direction. We have verified that a reduction of  $I_{\text{Kr}}$  was also unable to initiate unidirectional propagation.

We also investigated the effect of a discontinuity in conductivity between the M cell domain and the epicardium, as reported in a study.<sup>8</sup> We found that a large increase in resistance between the two domains could result in an extra stimulus in the epicardium that was provoked by an early after depolarization in the M cell domain. However, for the model used in our study, this increase was at least four times higher than the one reported in the literature. This indicates that the discontinuity in conductivity between the M cell domain and epicardium is likely insufficient to generate a premature stimulus arising from the M cell domain.

Our simulation study focused on early after depolarizations originating in M cells. We did not consider other possible sources of early after depolarizations. For example, cells in the right ventricular epicardium exhibit a prominent transient outward current  $I_{\text{to}}$ .<sup>35</sup> Early after depolarizations originating from the right ventricle epicardial cells might play a role in phase 2 reentry,<sup>36</sup> which is thought to be associated with the Brugada syndrome.<sup>37</sup> A recent numerical study, using a modified version of the LRd model that included  $I_{\text{to}}$  together with a large reduction in the time constant for the L type calcium channel, investigated this scenario.<sup>38</sup> These modifications were found, under very specific conditions, to elicit a secondary wave in a cable divided into two subdomains with different  $I_{\text{to}}$  densities. However, this scenario is specific to right ventricular epicardial cells and is unlikely to play a role in reentry phenomena associated with M cell domains in the left ventricle.

The second mechanism we investigated relies on the slow repolarization of the M cell domain which functions as a wave block for subsequent stimuli. When the M cell domain is inhomogeneous, or alternatively, if the pacing breaks the translational symmetry along the endocardial wall, a properly timed extra stimulus can be blocked in one area of the myocardium while allowed to propagate in another. This, then, could create reentrant excitation.

We first studied the propagation of stimuli, delivered prematurely with varying coupling intervals, for different basic cycle length and long QT syndrome strength. We found a rich set of possible dynamics of the wave following the premature stimulus. Particularly noteworthy was the dramatic reduction of the wave speed occurring within the M cell domain. Prerequisite for this behavior is a sufficiently long basic cycle length. Preliminary investigations of the dynamics indicate that during this slow propagation the usual sodium channel activation of neighboring cells fails. Instead, the calcium channel becomes responsible for the depolarization and the spread of the impulse. This scenario has also been observed experimentally in growth cultures of rat myocytes.<sup>39</sup>

The 1D simulations revealed two separate regions in the basic cycle length vs  $\mu$  space in which conduction block could occur. The first region, characterized by relatively

small basic cycle length, exhibits a small conduction block window. For coupling intervals within this window, the wave fails to propagate abruptly. The second region, characterized by a slow wave propagation and a subsequent wave block, has a much larger conduction block window. Furthermore, along the boundary of this region, the dynamics is not straightforward. A window of coupling intervals that exhibit conduction block is followed by a window of coupling intervals that show slow propagation within the M cell domain. Again, the calcium handling seems to be a likely candidate for an explanation of this behavior. This is supported by recent experimental work, able to visualize voltage and calcium simultaneously, that showed that calcium dynamics plays a crucial role in the generation of early after depolarizations in particular and action potential prolongation in general.<sup>40</sup> Thus, a model that faithfully incorporates calcium handling is essential. This might require a description of local spatial events including calcium sparks,<sup>41</sup> currently absent from the LRd model.

In mapping out the phase diagram of Fig. 9 we have focused on a point in the parameter space within this second region (basic cycle length of 1000 ms and  $\mu = 0.08$ ). The main finding of our 2D simulations is that the second mechanism can lead to reentrant excitations. Indeed, for large enough  $w$ , or large enough  $r$ , we find reentry that can last 1 s or more. The observed pseudo-ECG, with its polymorphic undulating morphology, is suggestive of torsade de pointes. Furthermore, for a large bubble size, the reentry becomes pinned to the region of heterogeneity, thus leading to long lasting reentrant excitations.

We should note that the observed mechanism for reentrant excitations is not specific to long QT 3. We have also investigated both the first and second mechanism in a model for long QT 2. In this model, we reduced the maximal conductance of  $I_{\text{Kr}}$  which allowed us to vary the strength of the long QT syndrome. As in our long QT 3 model, we found that early after depolarizations did occur in the M cell domain but were not able to excite neighboring tissue. On the other hand, when an M cell domain was included in the transmural sheet, the long QT 2 model was able to partially block a premature stimulus and sustained reentrant excitations were found. Also, we point out that we have replicated the pacing protocol employed in Ref. 11. There, the endocardium was paced at a long basic cycle length, followed by a premature stimulus on the epicardium. As the pacing protocol already breaks the translational symmetry along the endocardium, we included a continuous strip in our numerical geometry. We found that this pacing protocol could lead to reentry, provided that the strip had a sufficient width. Besides the geometrical construction of this paper or the pacing protocol of Ref. 11 there are other ways to break the translational symmetry. For example, a strip of M cells with domains of different long QT syndrome strength can have, for a given coupling interval, domains that exhibit wave block while other domains support normal propagation. This, again, would result in partial wave block and subsequent reentry.

The mechanism that was shown here to create reentrant excitation relies on an extra stimulus, delivered at a rela-

tively small coupling interval. This extra stimulus can possibly be generated by an early after depolarization in a Purkinje fiber that successfully excites the endocardium. A possible mechanism that would lead to the initiation of a wave originating from a Purkinje fiber early after depolarization is based on the experimentally observed reduced coupling between the Purkinje fiber and the endocardium.<sup>42</sup> Under this condition, numerical simulations have revealed that the inclusion of a large resistive barrier between the Purkinje fibers and the ventricular cells can lead to early after depolarizations in the Purkinje fibers that are able to generate extra stimuli in the ventricular domain.<sup>31</sup>

Our numerical simulations were carried out using a simplified transmural geometry of the ventricular wall that consisted of a centrally located M cell domain, sandwiched between two electrophysiologically equal domains representing the endo- and epicardium. Incorporating more realistic geometries and endo- and epicardial cells with different electrophysiological properties, however, will most likely not change the qualitative conclusions of this study. Furthermore, the action potentials of the epicardial and endocardial cells recorded in the wedge preparation of the canine left ventricle, were very similar.<sup>11</sup>

The numerical simulations employed 2D transmural sheets while the actual heart is of course a much more complicated 3D object. Nevertheless, our numerical work, replicating the experiments in wedges,<sup>11</sup> demonstrates that the creation of an intramural reentry event is plausible under certain conditions. In 3D, an ensuing intramural filament can either close on itself, leading to a scroll ring that remains intramural and is on the scale of the ventricles,<sup>43,44</sup> or can reorient and attach itself to the endo- and epicardium. Possible subsequent instabilities could destabilize this filament, resulting in multiple filaments and fibrillation. Only full-scale 3D simulations, preferably on realistic geometries containing detailed anatomical information, can address these events. We are currently investigating this possibility, which includes the development of novel algorithms that can accurately simulate electrical wave propagation in anatomically realistic hearts.<sup>45</sup>

## ACKNOWLEDGMENTS

The authors acknowledge support from the Whitaker Foundation and from the NSF sponsored Center for Theoretical Biological Physics (Grant Nos. PHY-0216576 and 0225630).

<sup>1</sup>Z. Qu, A. Garfinkel, P. S. Chen, and J. N. Weiss, "Mechanisms of discordant alternans and induction of reentry in simulated cardiac tissue," *Circulation* **102**, 1664–1670 (2000).

<sup>2</sup>M. A. Watanabe, F. H. Fenton, S. J. Evans, H. M. Hastings, and A. Karma, "Mechanisms for discordant alternans," *J. Cardiovasc. Electrophysiol.* **12**, 196–206 (2001).

<sup>3</sup>J. J. Fox, M. L. Riccio, F. Hua, E. Bodenschatz, and R. F. Gilmour, "Spatiotemporal transition to conduction block in canine ventricle," *Circ. Res.* **90**, 289–296 (2002).

<sup>4</sup>S. Sicouri and C. Antzelevitch, "A subpopulation of cells with unique electrophysiological properties in the deep subepicardium of the canine ventricle. The M cell," *Circ. Res.* **68**, 1729–1741 (1991).

<sup>5</sup>C. Antzelevitch, S. Sicouri, S. H. Litovsky, A. Lukas, S. C. Krishnan, J. M. D. Diego, G. A. Gintant, and D. W. Liu, "Heterogeneity within the

ventricular wall. Electrophysiology and pharmacology of epicardial, endocardial, and M cells," *Circ. Res.* **69**, 1427–1449 (1991).

<sup>6</sup>S. Sicouri, M. Quist, and C. Antzelevitch, "Evidence for the presence of M cells in the guinea pig ventricle," *J. Cardiovasc. Electrophysiol.* **7**, 503–511 (1996).

<sup>7</sup>E. Drouin, F. Charpentier, C. Gauthier, K. Laurent, and H. L. Marec, "Electrophysiologic characteristics of cells spanning the left ventricular wall of human heart: Evidence for presence of M cells," *J. Am. Coll. Cardiol.* **26**, 185–192 (1995).

<sup>8</sup>G. X. Yan, W. Shimizu, and C. Antzelevitch, "Characteristics and distribution of M cells in arterially perfused canine left ventricular wedge preparations," *Circulation* **98**, 1921–1927 (1998).

<sup>9</sup>C. Antzelevitch and J. Fish, "Electrical heterogeneity within the ventricular wall," *Basic Res. Cardiol.* **96**, 517–527 (2001).

<sup>10</sup>C. Antzelevitch and S. Sicouri, "Clinical relevance of cardiac arrhythmias generated by afterdepolarizations. Role of M cells in the generation of U waves, triggered activity and torsade de pointes," *J. Am. Coll. Cardiol.* **23**, 259–277 (1994).

<sup>11</sup>F. Akar, G. Yan, C. Antzelevitch, and D. Rosenbaum, "Unique topographical distribution of M-Cells underlies reentrant mechanism of torsade de pointes in the long QT syndrome," *Circulation* **105**, 1247–1253 (2002).

<sup>12</sup>C. Antzelevitch and W. Shimizu, "Cellular mechanisms underlying the long QT syndrome," *Curr. Opin. Cardiol.* **17**, 43–51 (2002).

<sup>13</sup>P. J. Schwartz, S. G. Priori, C. Spazzolini, A. J. Moss, G. M. Vincent, C. Napolitano, I. Denjoy, P. Guicheney, G. Breithardt, M. T. Keating, J. A. Towbin, A. H. Beggs, P. Brink, A. A. Wilde, L. Toivonen, W. Zareba, J. L. Robinson, K. W. Timothy, V. Corfield, D. Wattanasirichaigoon, C. Corbett, W. Haverkamp, E. Schulze-Bahr, M. H. Lehmann, K. Schwartz, P. Coumel, and R. Bloise, "Genotype-phenotype correlation in the long-QT syndrome: Gene-specific triggers for life-threatening arrhythmias," *Circulation* **103**, 89–95 (2001).

<sup>14</sup>C. Antzelevitch, "Sympathetic modulation of the long QT syndrome," *Eur. Heart J.* **23**, 1246–1252 (2002).

<sup>15</sup>A. T. Winfree, "Varieties of spiral wave behavior: An experimentalist's approach to the theory of excitable media," *Chaos* **1**, 303–334 (1991).

<sup>16</sup>W. Shimizu and C. Antzelevitch, "Sodium channel block with mexiletine is effective in reducing dispersion of repolarization and preventing torsade des pointes in LQT2 and LQT3 models of the long-QT syndrome," *Circulation* **96**, 2038–2047 (1997).

<sup>17</sup>P. C. Viswanathan and Y. Rudy, "Pause induced early afterdepolarizations in the long QT syndrome: A simulation study," *Cardiovasc. Res.* **42**, 530–542 (1999).

<sup>18</sup>C. E. Clancy and Y. Rudy, "Cellular consequences of HERG mutations in the long QT syndrome: Precursors to sudden cardiac death," *Cardiovasc. Res.* **50**, 301–313 (2001).

<sup>19</sup>P. C. Viswanathan and Y. Rudy, "Cellular arrhythmogenic effects of congenital and acquired long-QT syndrome in the heterogeneous myocardium," *Circulation* **101**, 1192–1198 (2000).

<sup>20</sup>K. Gima and Y. Rudy, "Ionic current basis of electrocardiographic waveforms: A model study," *Circ. Res.* **90**, 889–896 (2002).

<sup>21</sup>R. H. Clayton, A. Bailey, V. N. Biktashev, and A. V. Holden, "Re-entrant cardiac arrhythmias in computational models of long QT myocardium," *J. Theor. Biol.* **208**, 215–225 (2001).

<sup>22</sup>C. H. Luo and Y. Rudy, "A dynamic model of the cardiac ventricular action potential. I. Simulations of ionic currents and concentration changes," *Circ. Res.* **74**, 1071–1096 (1994).

<sup>23</sup>G. Faber and Y. Rudy, "Action potential and contractility changes in  $[Na^+]_i$  overloaded cardiac myocytes: a simulation study," *Biophys. J.* **78**, 2392–2404 (2000).

<sup>24</sup>M. Pressler, P. Münster, and X. Huang, *Cardiac Electrophysiology, From Cell to Beside, Gap Junction Distribution and Cardiac Conduction*, edited by D. P. Zipes and J. Jalife, 2nd ed. (Saunders, Philadelphia, 1995), Chap. 16, pp. 144–145.

<sup>25</sup>C. H. Luo and Y. Rudy, "A model of the ventricular cardiac action potential. Depolarization, repolarization, and their interaction," *Circ. Res.* **68**, 1501–1526 (1991).

<sup>26</sup>G. W. Beeler and H. Reuter, "Reconstruction of the action potential of ventricular myocardial fibres," *J. Physiol. (London)* **268**, 177–210 (1977).

<sup>27</sup>J. J. Fox, J. L. McHarg, and R. F. Gilmour, "Ionic mechanism of electrical alternans," *Am. J. Physiol. Heart Circ. Physiol.* **282**, H516–H530 (2002).

<sup>28</sup>C. E. Clancy and Y. Rudy, "Linking a genetic defect to its cellular phenotype in a cardiac arrhythmia," *Nature (London)* **400**, 566–569 (1999).

<sup>29</sup>C. E. Clancy and Y. Rudy, "Na<sup>+</sup> channel mutation that causes both Bru-

- gada and long-QT syndrome phenotypes: A simulation study of mechanism," *Circulation* **105**, 1208–1213 (2002).
- <sup>30</sup>J. Saiz, J. Ferrero, M. Monserrat, J. Ferrero, and N. Thakor, "Influence of electrical coupling on early afterdepolarizations in ventricular myocytes," *IEEE Trans. Biomed. Eng.* **46**, 138–147 (1999).
- <sup>31</sup>M. Monserrat, J. Saiz, J. Ferrero, J. Ferrero, and N. Thakor, "Ectopic activity in ventricular cells induced by early afterdepolarizations developed in Purkinje cells," *Ann. Biomed. Eng.* **28**, 1343–1351 (2000).
- <sup>32</sup>R. H. Clayton, K. Parkinson, and A. V. Holden, "Re-entry in computational models of ischaemic myocardium," *Chaos, Solitons Fractals* **13**, 1671–1683 (2002).
- <sup>33</sup>R. Plonsey and R. Barr, *Bioelectricity: A Quantitative Approach* (Plenum, New York, 1988).
- <sup>34</sup>C. H. Luo and Y. Rudy, "A dynamic model of the cardiac ventricular action potential. II. Afterdepolarizations, triggered activity, and potentiation," *Circ. Res.* **74**, 1097–1113 (1994).
- <sup>35</sup>J. M. D. Diego, Z. Q. Sun, and C. Antzelevitch, " $I_{to}$  and action potential notch are smaller in left vs. right canine ventricular epicardium," *Am. J. Physiol.* **271**, H548–H561 (1996).
- <sup>36</sup>A. Lukas and C. Antzelevitch, "Phase 2 reentry as a mechanism of initiation of circus movement reentry in canine epicardium exposed to simulated ischemia," *Cardiovasc. Res.* **32**, 593–603 (1996).
- <sup>37</sup>C. Antzelevitch, P. Brugada, J. Brugada, R. Brugada, J. A. Towbin, and K. Nademanee, "Brugada syndrome: 1992–2002: A historical perspective," *J. Am. Coll. Cardiol.* **41**, 1665–1671 (2003).
- <sup>38</sup>S. Miyoshi, H. Mitamura, K. Fujikura, Y. Fukuda, K. Tanimoto, Y. Hagiwara, M. Ita, and S. Ogawa, "A mathematical model of phase 2 reentry: Role of 1-type Ca current," *Am. J. Physiol. Heart Circ. Physiol.* **284**, H1285–H1294 (2003).
- <sup>39</sup>S. Rohr and J. P. Kucera, "Involvement of the calcium inward current in cardiac impulse propagation: Induction of unidirectional conduction block by nifedipine and reversal by Bay K 8644," *Biophys. J.* **72**, 754–766 (1997).
- <sup>40</sup>B. R. Choi, F. Burton, and G. Salama, "Cytosolic Ca<sup>2+</sup> triggers early afterdepolarizations and torsade de pointes in rabbit hearts with type 2 long QT syndrome," *J. Physiol. (London)* **543**, 615–631 (2002).
- <sup>41</sup>D. Bers, *Excitation–Contraction Coupling and Cardiac Contractile Force* (Kluwer, Boston, 2001).
- <sup>42</sup>D. A. Rawling and R. W. Joyner, "Characteristics of junctional regions between Purkinje and ventricular muscle cells of canine ventricular sub-endocardium," *Circ. Res.* **60**, 580–585 (1987).
- <sup>43</sup>N. El-Sherif, E. B. Caref, H. Yin, and M. Restivo, "The electrophysiological mechanism of ventricular arrhythmias in the long QT syndrome. Tridimensional mapping of activation and recovery patterns," *Circ. Res.* **79**, 474–492 (1996).
- <sup>44</sup>S. C. Verduyn, M. A. Vos, J. van der Zande, F. F. van der Hulst, and H. J. Wellens, "Role of interventricular dispersion of repolarization in acquired torsade-de-pointes arrhythmias: Reversal by magnesium," *Cardiovasc. Res.* **34**, 453–463 (1997).
- <sup>45</sup>E. M. Cherry, W.-J. Rappel, S. Evans, and F. Fenton, "Effects of wall heterogeneity in an anatomically realistic model of canine ventricles: A simulation study," *PACE* **26**, 1109–1109 (2003).